SUPPORTING INFORMATION

Ligating Dopamine as Signal Trigger onto the Substrate *via* Metal-Catalyst-Free Click Chemistry for "Signal-on" Photoelectrochemical Sensing of Ultralow MicroRNA Levels

Cui Ye[†], Min Qiang Wang[‡], Zhong Feng Gao[†], Ying Zhang[†], Jing Lei Lei[ǂ], Hong Qun Luo[*†], and Nian Bing Li[*†]

[†] Key Laboratory of Eco-environments in Three Gorges Reservoir Region (Ministry of Education), School of Chemistry and Chemical Engineering, Southwest University, Chongqing 400715, People's Republic of China
[‡] Institute for Clean Energy & Advanced Materials, Faculty of Materials and Energy, Southwest University, Chongqing 400715, People's Republic of China
[ǂ] School of Chemistry and Chemical Engineering, Chongqing University, Chongqing 400044, People's Republic of China

[*] Corresponding author. Tel: +86 23 68253237; Fax: +86 23 68253237;
E–mail address: linb@swu.edu.cn (N. B. Li), luohq@swu.edu.cn (H.Q. Luo)

Contents

Chemicals and Reagents. All oligonucleotides were synthesized and purified by Sangon Inc. (Shanghai, China), and the sequences are shown in Table 1. 2-Amino-2-(hydroxymethyl)-1,3-propanediol (Tris), 6-mercaptohexanol (MCH), $HAuCl_4 \cdot 4H_2O$, (1-ethyl-3-[3-dimethylaminopropyl]carbodiimide hydrochloride) (EDC), N-hydroxysuccinimide (NHS), dopamine (DA), L-cysteine (L-cys), histidine (His), L-glutathione oxidized (GSSG), and Tris(2-carbozyethyl)phosphine hydrochloride (TCEP) were purchased from Sigma-Aldrich (St. Louis, MO), and used without further purification. Other reagents of analytical reagent grade were purchased from Chengdu Kelong Chemical Reagents Factory (Chengdu, China) and used as received. All solutions were prepared by ultrapure water with a resistivity of 18.2 MΩ cm. The experiment temperature was kept with an SD-101-005DB super digital thermostat bath purchased from Sida Experimental Equipment Ltd., Chongqing, China. The colloidal gold nanoparticles (GNPs) were prepared by reducing $HAuCl_4$ (1 wt.%) with 2.2 mM sodium citrate at 100 °C for half an hour. Ferricyanide solution ($Fe(CN)_6^{3-/4-}$, 5 mM) was obtained by dissolving potassium ferricyanide and potassium ferrocyanide in 0.1 M phosphate buffer (0.1 M KCl, 0.1 M KH_2PO_4, 0.1 M Na_2HPO_4, pH 7.4).

Table S1. Sequence Information for the Nucleic Acids Used in This Study.

Name	Sequence (5′−3′)
MiRNA-141	UAA CAC UGU CUG GUA AAG AUG G
miR-200a	UAACACUGUCUGGUAACGAUGU.
miR-200b	UAAUACUGCCUGGUAAUGAUGA.
miR-200c	UAAUACUGCCGGGUAAUGAUGGA
miR-429	UAAUACUGUCUGGUAAAACCGU
Tetrahedron A	ACATTCCTAAGTCTGAAACATTACAGCTTGCTACACGAGAAGAGCCGCCATAGTATTAGCT CACCATCTTTACTGAGCT
Tetrahedron B	SH-C_6-TATCACCAGGCAGTTGACAGTGTAGCAAGCTGTAATAGATGCGAGGGTCCAATAC
Tetrahedron C	SH-C_6-TCAACTGCCTGGTGATAAAACGACACTACGTGGGAATCTACTATGGCGGCTCTTC
Tetrahedron D	SH-C_6-TTCAGACTTAGGAATGTGCTTCCCACGTAGTGTCGTTTGTATTGGACCCTCGCAT
H1	TTATGAGCTATATTGAAACAGCTCATAACACTGTCTGA-DBCO
H2	DBCO-GTTTCAATATAGCTCATAATCAGACAGTGTTATGAGCT
H1’	COOH-TTATGAGCTATATTGAAACAGCTCATAACACTGTCTGA
H2’	COOH-GTTTCAATATAGCTCATAATCAGACAGTGTTATGAGCT
Probe-N_3	COOH-AGAGCGA-N_3

Apparatus. The morphologies and structures were respectively characterized by field-emission scanning electron microscopy (FESEM) with JEOL-7800F and energy-dispersive X-ray spectroscopy (EDS) with INCA X-Max 250 (Japan Electron Optics Laboratory Co., Japan). The transmission electron microscopy (TEM) image was obtained using a JEM-2100 (TEM, JEOL-2100, Japan) equipped with a field emission gun (FEG) at 200 kV. The X-ray diffraction pattern (XRD) was investigated by an XRD-7000 with Cu Kα source radiation at a scanning rate of 2° min^{-1} from 10° to 80° (Shimadzu, Japan). X-ray photoelectron spectroscopy (XPS) analysis was obtained on the Thermo ESCALAB 250Xi spectrometer with Al Ka X-ray (1486.6 eV) as the light source

(Thermoelectricity Instruments, USA). PEC measurements were carried out with PEAC 200A (Tianjin AiDa Hengsheng Technology Co., Ltd., China). Electrochemical measurements were recorded on a CHI 660D electrochemical workstation (Shanghai Chenhua Instruments Co., China). And the three-electrode cell contains a modified glassy carbon electrode (GCE, Φ = 3 mm) as the working electrode, an Ag/AgCl for PEC measurements or a saturated calomel electrode (SCE) for electrochemical measurements as the reference electrode, and a platinum wire as the counter electrode.

Preparation of Bi_2S_3@MoS_2 Nanoflowers. The Bi_2S_3@MoS_2 nanoflowers were synthesized by a solvothermal technique. Briefly, 0.97 g of $Bi(NO_3)_3 \cdot 5H_2O$ and 0.456 g of thiourea were dissolved in a 50 mL mixture of ultrapure water and ethylene glycol (EG) with a volume ratio of $V_{H_2O} : V_{EG} = 1:4$. Then, the resultant homogeneous solution was transferred to a 100 mL Teflon-lined stainless-steel autoclave, and the autoclave was heated at 140 °C for 1 h, followed by cooling to room temperature. The products were separated centrifugally, washed with ultrapure water and ethanol for several times, and dried under vacuum. Subsequently, 0.1 g of Bi_2S_3 powder was ultrasonically dispersed in 10 mL of ultrapure water. 0.075 g of $Na_2MoO_4 \cdot 2H_2O$ and 75 μL of PDDA (20 wt.%) were added to above Bi_2S_3 dispersion. Next, 0.2 g of thiourea was added to the mixture, and then the mixture was diluted to 20 mL under vigorously stirring for 1 h. Finally, the obtained solution was maintained at 200 °C for 24 h in a 30 mL Teflon-lined stainless-steel autoclave. After cooling to room temperature, the black products were separated centrifugally, washed with ultrapure water and ethanol for several times, and dried under vacuum.

Self-Assembly of Tetrahedral DNA Nanostructure at the Modified Electrode. The tetrahedral DNA nanostructure consisted of four DNA strands was formed based on a modified protocol.[1,2] Tetrahedron A, B, C, and D were separately dissolved in TM buffer (10 mM Tris-HCl, 50 mM $MgCl_2$, pH 8.0), yielding a final concentration of 50 μM. Each strand (2 μL) was mixed with TCEP (10 μL, 30 mM) and 82 μL of TM buffer. Afterward, the resulting mixture was heated to 95 °C for 2 min and then cooled to 4 °C. The final concentration of tetrahedron-structured probe (TSP) is 1 μM. Prior to surface modification, the GCE was polished with alumina slurry, followed by sonicating in anhydrous ethanol and ultrapure water. The well-polished bare GCE was first coated with as-prepared Bi_2S_3@MoS_2 nanoflowers dispersion (4 μL, 2 mg mL^{-1}) and evaporated in air. The Bi_2S_3@MoS_2 nanocomposites on the GCE would turn into stable film used as the substrate of the PEC biosensor, and then the colloidal GNPs were adsorbed on the composite by immersing

Bi_2S_3@MoS_2/GCE into a colloidal GNPs solution for 8 h. After being rinsed and dried, 10 μL of TSP was added to the modified electrode surface and allowed to react overnight at room temperature.

Preparation of Signal Probe. First, the ligation probe probe-N_3 (10 μL, 100 μM) was added to 240 μL of a mixture of EDC and NHS (4:1) and then stirred over 12 h to activate the carboxyl at room temperature. Subsequently, DA (250 μL, 20 mM) was added to the obtained probe-N_3 mixture, simultaneously stirring for 2 h to obtain the signal probe (P_{DA}-N_3, 2 μM probe-N_3, 10 mM DA) *via* amidation reaction.

CV and PEC Characterization of the PEC Biosensor. To confirm the fabrication process of the PEC biosensor, the electrochemical characterization of the stepwise-modified electrode was executed by cyclic voltammograms (CVs) in 5.0 mM $[Fe(CN)_6]^{3-/4-}$ solution. As shown in Figure S1A, a couple of quasi-reversible redox peaks are obtained at the bare GCE (curve a). After being modified with the Bi_2S_3@MoS_2 nanoflowers on the bare GCE surface, an obvious decrease in redox peak current is achieved (curve b). Then GNPs are introduced onto the electrode, and the redox peak current is enhanced, indicating that GNPs provide excellent conductivity and large surface area to promote the electron transfer (curve c). When the thiol-modified TSP is fabricated on the electrode with the help of GNPs, an obviously decreased peak current is observed due to its feature of obstructing the electron transfer (curve d). Followed by employing MCH to block nonspecific binding sites, a successive decline is obtained (curve e). The current further decreases after immobilizing target successfully (curve f), which is attributed to the hindrance of the electron transfer. As expected, when the modified electrode is incubated sequentially with H1, H2, and P_{DA}-N_3, the currents still decline (curves g, h).

The fabrication process of the PEC biosensor can also be studied by monitoring the photocurrent response, as shown in Figure S1B. A low background photocurrent is observed at the bare GCE (curve a). Then the Bi_2S_3@MoS_2/GCE yields a significantly enhanced photocurrent (curve b) because the composite nanoflowers with the unique structure of MoS_2 nanosheet-coated Bi_2S_3 nanoflowers exhibit photoactivity enhancement under a visible-light ($\lambda > 400$ nm) illumination, resulting in high photon-to-electron conversion efficiency. After GNPs immobilization, the photocurrent evidently increases (curve c), because of the surface plasmon resonance (SPR) effect of GNPs, which increases the light absorption and enhances the charge separation. Moreover, GNPs can significantly enhance electrical conductivity, thus resulting in the obvious enhancement of photocurrent. The photocurrent decreases followed by the TSP and MCH immobilization (curves d,

e), and the photocurrent further decreases after the target is incubated (curve f). When H1 and H2 are bound by the HCR reaction, the photocurrent decreases moderately (curve g). The decrease in photocurrent intensity can be explained by increasing the steric-hindrance effect and decreasing the electron-transfer efficiency. Lastly, the P_{DA}-N_3 is labeled to hybridize via CC, and the photocurrent increases remarkably (curve h), which is attributed to the introduction of the electron donor DA acting as a captor of photo-generated holes. Thus, all of these results demonstrate the successful fabrication of the PEC biosensor.

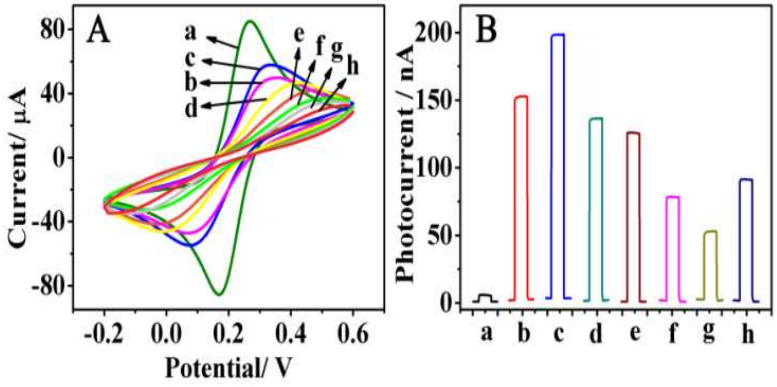

Figure S1. (A) CV profiles in 5.0 mM $[Fe(CN)_6]^{3-/4-}$ at a scan rate of 50 mV/s and (B) photocurrent responses toward 0.5 nM miRNA of the prepared biosensor at the (a) bare GCE, (b) Bi_2S_3@MoS_2/GCE, (c) GNPs/Bi_2S_3@MoS_2/GCE, (d) TSP/GNPs/Bi_2S_3@MoS_2/GCE, (e) MCH/TSP /GNPs/Bi_2S_3@MoS_2/GCE, (f) miRNA/MCH/TSP/GNPs/Bi_2S_3@MoS_2/GCE, (g) H1, H2/miRNA /MCH/TSP/GNPs/Bi_2S_3@MoS_2/GCE, (h) P_{DA}-N_3/H1, H2/miRNA/MCH/TSP/GNPs/Bi_2S_3@MoS_2/GCE.

Experimental Details for the Optimal Analytical Performance of the PEC Biosensor. To achieve an optimal analytical performance of the PEC biosensor, several experimental conditions were investigated. As a PEC detection protocol, we first screened the alternatives of electron donors that may affect the electron-hole recombinant. We selected these substances including dopamine (DA), L-cysteine (L-cys), histidine (His), L-glutathione oxidized (GSSG), and respectively synthesized signal probes P_{DA}-N_3, $P_{L\text{-}cys}$-N_3, P_{His}-N_3, and P_{GSSG}-N_3 (detailed synthesis method seen in the section of Preparation of Signal Probe). The photocurrent intensity of the resulting electrodes (detailed description about the construction of the resulting electrodes seen in the section of Self-Enhanced PEC Biosensor for MiRNA Assay) P_X-N_3/H1, H2/miRNA/MCH/TSP/GNPs/Bi_2S_3 @ MoS_2/GCE (X= DA, L-cys, His, and GSSG) were recorded in 0.1 mol L^{-1} phosphate buffer (pH 7.4) irradiated with a visible-light.

The hybridization time of HCR was evaluated by using the photocurrent response. When we constructed the resulting electrodes P_{DA}-N_3/H1, H2/miRNA/MCH/TSP/GNPs/Bi_2S_3 @ MoS_2/GCE, the electrodes were respectively incubated with the mixture of 10 μL of H1 and 10 μL of H2 for 0.5,

1, 1.5, 2, 2.5 and 3 h to fulfill the HCR. The photocurrent intensity of the resulting electrodes was recorded in 0.1 mol L^{-1} phosphate buffer (pH 7.4) irradiated with a visible-light. The reaction time of CC was also investigated. Similarly, when we constructed the resulting electrodes P_{DA}-N_3/H1, H2/miRNA/MCH/TSP/GNPs/Bi_2S_3 @ MoS_2/GCE, the electrode was dipped with 20 μL of P_{DA}-N_3 at room temperature for 5, 10, 15, 20, 25, and 30 min incubation to fulfill the CC reaction. The photocurrent intensity of the resulting electrodes was recorded in 0.1 mol L^{-1} phosphate buffer (pH 7.4) irradiated with a visible-light.

The concentration of DA was evaluated which is expected to affect the response signal. When we synthesize the signal probe P_{DA}-N_3 (detailed synthesis method is seen in the section of Preparation of Signal Probe), the final concentration of DA in P_{DA}-N_3 was optimized, including 1, 5, 7.5, 10, 30, and 50 mM. The photocurrent intensity of the resulting electrodes P_{DA}-N_3/H1, H2/miRNA/MCH/TSP/GNPs/Bi_2S_3 @ MoS_2/GCE was recorded in 0.1 mol L^{-1} phosphate buffer (pH 7.4) irradiated with a visible-light. Meanwhile, the effect of different introduction methods, such as CC and covalent bonding, of electron donor DA was investigated. Two kinds of trapped hairpins (H1, H2 and H1', H2') were designed. H1 and H2 modified DBCO can ligate P_{DA}-N_3 *via* CC to efficiently introduce DA. H1' and H2' modified COOH can introduce DA *via* covalent bonding. In our work, HCR was executed, and then P_{DA}-N_3 was ligated into the substrate. The resulting electrode was abbreviated as P_{DA}-N_3/H1, H2/miRNA/MCH/TSP/GNPs/Bi_2S_3 @ MoS_2/GCE. In the control experiment, after HCR of H1' and H2', amidation reaction of DA with COOH groups at H1' and H2' was carried out. The resulting electrode was abbreviated as DA/H1', H2'/miRNA/MCH/TSP/GNPs/Bi_2S_3 @ MoS_2/GCE. The photocurrent intensity of those two kinds of resulting electrodes was recorded in 0.1 mol L^{-1} phosphate buffer (pH 7.4) irradiated with a visible-light.

Contribution of HCR to Signal Amplification. To clarify the contribution of HCR to signal amplification, control experiment has been executed by using H1 only for miRNA detection, and the resulting electrode was abbreviated as P_{DA}-N_3/H1/miRNA/MCH/TSP/GNPs/Bi_2S_3@MoS_2/GCE. As shown in Figure S2, the photocurrent of the proposed biosensor in our work (curve b) is obviously higher than that of the sensor in the control experiment (curve a). Thus, HCR is vital to signal amplification in this proposed method.

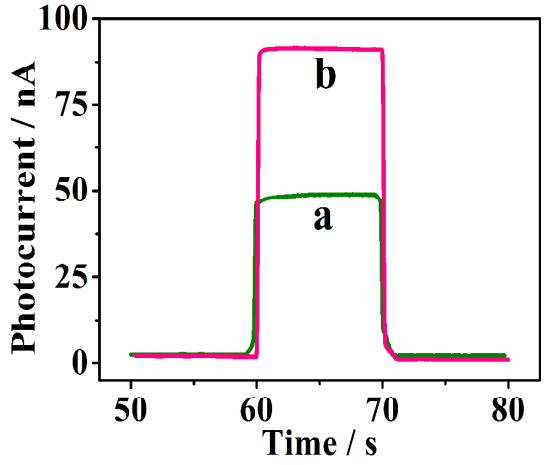

Figure S2. Photocurrent responses toward 0.5 nM miRNA at the (a) P_{DA}-N_3/H1/miRNA/MCH/TSP/GNPs/Bi_2S_3@MoS_2/GCE, and (b) P_{DA}-N_3/H1,H2/miRNA/MCH/TSP/GNPs/Bi_2S_3@MoS_2/GCE.

Effect of the Amount of TSP. The amount of TSP immobilized onto the surface of electrodes was optimized. The photocurrent response of the resulting electrodes was measured by incubating different amounts of TSP. As illustrated in Figure S3, the photocurrent increases with the augment of the amount of TSP. When the amount of TSP reaches 10^{-11} mol (1 μM 10 μL), the photocurrent levels off. Considering the photocurrent intensity and the consumption of the reagents, 10^{-11} mol (1 μM 10 μL) was chosen as the optimal amount of TSP.

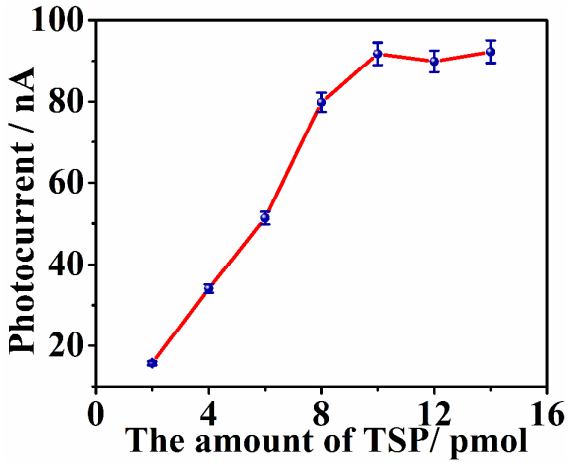

Figure S3. Effect of the amount of TSP at P_{DA}-N_3/H1, H2/miRNA/MCH/TSP/GNPs/Bi_2S_3@MoS_2/GCE.

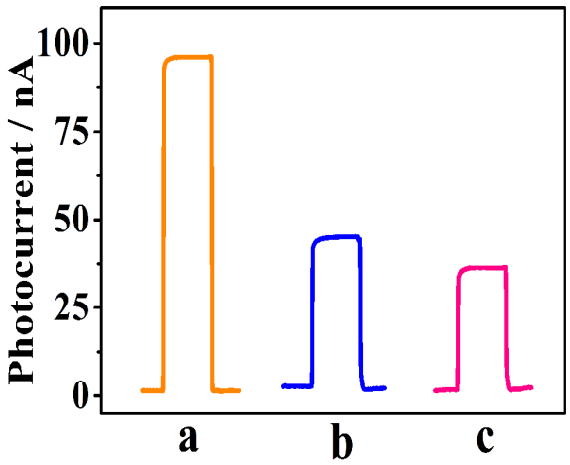

Figure S4. Photocurrent responses toward 0.5 nM miRNA at the (a) P_{DA}-N_3/H1, H2/miRNA/MCH/TSP/GNPs/Bi_2S_3@MoS_2/GCE, (b) P_{DA}-N_3@H1, P_{DA}-N_3@H2/miRNA/MCH/TSP/GNPs/Bi_2S_3 @ MoS_2/GCE, and (c) DA@H1', DA@H2'/miRNA/MCH/TSP/GNPs/Bi_2S_3 @ MoS_2/GCE.

Certification of the Rational Design to Conduct CC after HCR. To certify the rational design of conduct CC after HCR, control experiments were executed. First, two kinds of signal probes were synthesized. H1 and H2 respectively reacted with P_{DA}-N_3 *via* CC to obtain signal probes P_{DA}-N_3@H1 and P_{DA}-N_3@H2. H1' and H2' respectively reacted with DA *via* amidation reaction to obtain signal probes DA@H1' and DA@H2'. Then those two kinds of resulting electrodes were constructed and abbreviated severally as P_{DA}-N_3@H1, P_{DA}-N_3@H2/miRNA/MCH/TSP/GNPs/Bi_2S_3 @ MoS_2/GCE and DA@H1', DA@H2'/miRNA/MCH/TSP/GNPs/Bi_2S_3 @ MoS_2/GCE. In our work, the resulting electrode was abbreviated as P_{DA}-N_3/H1, H2/miRNA/MCH/TSP/GNPs/Bi_2S_3 @ MoS_2/GCE. As shown in Figure S4, the photocurrent response of curve a is much higher than that of curve b and curve a, thus certifying the rational design of conduct CC after HCR.

Table S2. Comparison with Reported MiRNA Detection Methods.

Method	Detection limit (fM)	Dynamic range (fM - nM)	Analysis time (h)	Ref
Photoluminescence	3800	3800 – 10	7	3
Photoluminescence	1.0	1.0 – 1.0	>24	4
Electrochemistry	0.1	0.1 – 0.5	22	5
Electrochemistry	0.4	1.0 – 1.0	12	6
ECL	0.5	1.0 – 1.0	5	7
ECL	–	1.0 – 0.01	-	8
PEC	1.7	5.0 – 0.005	9.25	9
PEC	0.027	0.1 – 0.5	5.25	This work

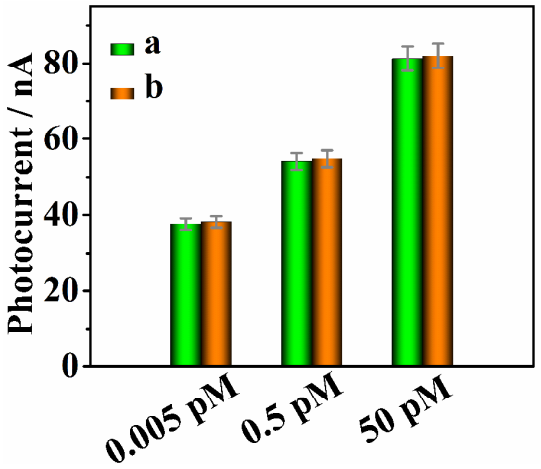

Figure S5. Photocurrent responses of the proposed biosensor towards 0.005, 0.5, and 50 pM miRNA in (a) TM buffer solution and (b) lysates from 10^2 cells of HeLa.

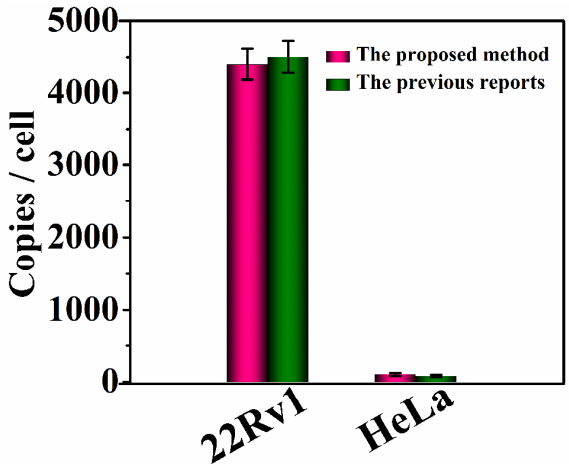

Figure S6. The number of copies of miRNA-141 per cell determined using our proposed method in 22Rv1 cell and HeLa cell compared with the previous reports.[10,11]

References

(1) Lin, M.; Wen, Y.; Li, L.; Pei, H.; Liu, G.; Song, H.; Zuo, X.; Fan, C.; Huang, Q. *Anal. Chem.* **2014**, *86*, 2285-2288.
(2) Sadowski, J. P.; Calvert, C. R.; Zhang, D. Y.; Pierce, N. A.; Yin, P. *ACS Nano* **2014**, *8*, 3251-3259.
(3) Wang, W.; Kong, T.; Zhang, D.; Zhang, J. N.; Cheng, G. S. *Anal. Chem.* **2015**, *87*, 10822-10829.
(4) Causa, F.; Aliberti, A.; Cusano, A. M.; Battista, E.; Netti, P. A. *J. Am. Chem. Soc.* **2015**, *137*, 1758-1761.
(5) Wang, T. Y.; Viennois, E.; Merlin, D.; Wang, G. L. *Anal. Chem.* **2015**, *87*, 8173-8180.
(6) Miao, P.; Wang, B. D.; Chen, X. F.; Li, X. X.; Tang, Y. G. *ACS Appl. Mater. Interfaces* **2015**, *7*, 6238-6243.
(7) Feng, Q. M.; Shen, Y. Z.; Li, M. X.; Zhang, Z. L.; Zhao, W.; Xu, J. J.; Chen, H. Y. *Anal. Chem.* **2016**, *88*, 937-944.
(8) Liao, Y. H.; Huang, R.; Ma, Z. K.; Wu, Y. X.; Zhou, X. M.; Xing, D. *Anal. Chem.* **2014**, *86*, 4596-4604.
(9) Wang, M.; Yin, H. S.; Shen, N. N.; Xu, Z. N.; Sun, B.; Ai, S. Y. *Biosens. Bioelectron.* **2014**, *53*, 232-237.
(10) Liu, Y. Q.; Zhang, M.; Yin, B. C.; Ye, B. C. *Anal. Chem.* **2012**, 84, 5165-5169.
(11) He, X. W.; Zeng, T.; Li, Z.; Wang, G. L.; Ma, N. *Angew. Chem. Int. Ed.* **2015**, 54, 1-5.